Journal of Constructional Steel Research 188 (2022) 107002

Contents lists available at ScienceDirect

Journal of Constructional Steel Research

journal homepage: www.elsevier.com/locate/jcsr

# Flexural buckling of stainless steel CHS columns: Reliability analysis utilizing FEM simulations

Daniel Jindra *, Zdeněk Kala, Jiří Kala

*Faculty of Civil Engineering, Brno University of Technology, Veveří 331/95, 602 00 Brno, Czech Republic*

ARTICLE INFO

*Keywords:*
Stainless steel
Flexural buckling
Circular hollow section (CHS)
Finite element modelling (FEM)
First order reliability method
Design methods

ABSTRACT

This paper presents a numerical investigation of the ultimate limit state of imperfect columns under axial compression; the columns are made of stainless steel with a circular hollow cross-section (CHS). The subject of interest is the statistical analysis of the ultimate resistance. Statistical characteristics of input material and geometric imperfections are taken from the results of experimental research published in the literature. The first-order reliability method (FORM) along with geometrically and materially nonlinear imperfect numerical analysis (GMNIA) is conducted. The ultimate resistances of CHS columns in flexural buckling obtained from the finite element analyses are compared with the design resistances based on the corresponding European standard, considering various slenderness values. Two approaches of the initial geometrical imperfection amplitude consideration are presented. The influence of correlation between the ultimate resistance of stainless steel columns in compression and input parameters is discussed, with a focus on the geometrical imperfection influence. The results may be useful for the verification of the European standard where the flexural buckling curves of stainless steel columns are relatively new and thus are based on a relatively weaker theoretical and experimental basis compared to carbon steel.

## 1. Introduction

Round tubular steel sections also commonly known as circular hollow sections (CHS) are popular due to their multi-purpose possibilities in civil engineering. The uniform distribution of the material within the section around the polar axis increases the torsional resistance, improves the bi-axial bending resistance, and minimizes the exposed external area, therefore reducing maintenance requirements. The possibilities of CHS applications for engineering purposes are numerous, from more common structural members to composite steel-concrete members used, e.g., in offshore structures [1].

The material of stainless steel was first introduced as “rustless steel” in 1912–1913 [2], and ever since the popularity of this material has been rising. The most frequently used grades of the stainless steel materials are ferritic, austenitic, and duplex; all differing in chemical composition (most importantly in the content of chromium and nickel) [2]. The corrosion resistance is convenient for various facade applications of this material, e.g., in Nascar Hall of Fame (2010), in Charlotte, North Carolina, U.S., Museum of Contemporary Art (2012), Cleveland, U.S., or Investcorp Building at St. Anthony’s College (2015), Oxford, U.K. From the structural engineering point of view, a more suitable use of this material for load-bearing members is involved, e.g., in the composite duplex stainless-steel arch bridge in Cala Galdana on the island of Menorca, Spain (2005) [3], or in the UK’s first stainless-steel vehicular bridge in Pooley Bridge (2020). The use of stainless steel is cost-effective in structures exposed to aggressive environments [4], e.g., in the construction of bridges or offshore structures. Recently, even methods of additive manufacturing (also referred to as 3D printing) have been experimentally and numerically investigated. The cross-sectional behaviour of CHS produced by powder bed fusion (PBF) from Grade 316 L stainless steel powder is presented in a study by Zhang et al. [5].

Several recent studies of the stainless steel CHS members in buckling deal with the fire resistance performance of these members, e.g., the study by He et al. [6], Martins et al. [7], Mohammed and Cashell [8], or by Mohammed and Afshan [9] who investigated not only CHS but also SHS and RHS (square and rectangular hollow section, respectively). Residual strengths of stainless steel CHS columns after fire exposure were studied by He et al. [10]. These studies [6–10] concluded that, for a significant fraction of specimens, the design rules of the appropriate European standard (EC 3) [11] provide rather scattered and often unsafe

* Corresponding author.
*E-mail address:* jindra.d@fce.vutbr.cz (D. Jindra).

https://doi.org/10.1016/j.jcsr.2021.107002
Received 10 August 2021; Received in revised form 10 October 2021; Accepted 14 October 2021

predictions of flexural buckling strengths for stainless steel CHS members after fire exposure.

Not only might the standardized design not be conservative enough under extreme loading conditions, but the EC3 [11] design methods are unsafe in predicting the flexural buckling resistance of CHS members for certain slenderness values in general, as has already been pointed out in several studies, e.g., by Young and Hartono [12], Rasmussen and Rondal. [13], Ashraf et al. [14], Theofanous et al. [15], Shu et al. [16] or Young and Ellobody [17,18]. Also, the flexural buckling performance of hot-rolled duplex stainless steel CHS columns has been recently investigated using a comprehensive experimental and numerical program by Ning et al. [19], with the same conclusion, which was mainly caused by a lack of appropriate CHS experimental data at the creation time of the corresponding EC 3 standard [13]. Mainly RHS and SHS experimental data were considered for the EN flexural buckling curve calibration, however, increased material strength in hardened corner areas of the RHS and SHS profiles resulted in an overall different performance compared to that in CHS sections [20]. The current stainless steel production technology is different and generally better than the former carbon steel technology. Also, the technology of stainless steel production has been improving over the last decade, and this might influence the coefficients utilized in the current design approach especially for short bars where buckling does not play an important role. Therefore, the current design approach of stainless steel members per the EC 3 standard [11] still requires more precise calibration of the coefficients utilized throughout the design process itself, such as the partial safety factors, or more suitable values of limit slenderness (which is the main objective of this study), or various other coefficients to sustain the required level of structural reliability.

Existing test results of the stainless steel CHS members in compression have been documented, e.g., by Rasmussen and Hancock [21], Talja [22], Burgan et al. [23], Rasmussen [24], Kuwamura [25], Gardner and Nethercot [26], Lam and Gardner [27], Uy et al. [28], or Zhao et al. [29,30]. The major focus of these researchers was predominantly on austenitic grades of stainless steel stub column results. The duplex grade of stainless steel CHS stub column tests were conducted, e.g., by Bardi and Kyriakides [31], or Paquette and Kyriakides [32], while the ferritic material was tested by Stangenberg [33]. Comprehensive experimental and numerical studies of different CHS columns in compression of a wide range of member slenderness (considering several material grades) were carried out by Buchanan et al. [34]. Loading eccentricities of the CHS members exposed to flexural buckling were later introduced and investigated in detail in a subsequent study of Buchanan et al. [35].

Several design provisions in CHS member compression capacity were recommended. Different flexural buckling curve alternations were proposed, e.g., by Rasmussen and Rondal [13], Theofanous et al. [15], Young and Ellobody [17], or Buchanan et al. [34]. In a recent study by Xu et al. [36], a machine learning algorithm was adopted to develop a unified design method suitable for various stainless steel grades and failure modes of CHS columns. Another unified approach for assessing the structural behaviour of austenitic and ferritic stainless steel CHS columns under eccentric loading was proposed by Ma et al. [37].

In this paper, failure due to flexural buckling of austenitic stainless steel CHS columns is being investigated using advanced numerical geometrically and materially nonlinear analyses with imperfections (GMNIA) using the ANSYS software [38]. The first-order reliability method (FORM) by the European standard EN 1990-1-1 [39] is conducted to obtain the flexural buckling design resistances based on the finite element analyses. The required statistical values of material parameters are adopted in accordance with the recent statistical research of stainless steel members by Arrayago et al. [40].

The ultimate design resistances of CHS columns in flexural buckling obtained from the advanced numerical analyses are compared with the design resistances based on EN 1993-1-4 [11], for different slenderness values. Moreover, the EN design resistance with consideration of the conditions for the flexural buckling curve proposed by Buchanan et al. [34] is discussed. This design provision was chosen by researchers from the available ones [13,15,17,36,37] based on its very simple utilization and probably the most feasible possibility of future implementation into the current European standard EC 3 [11].

Two approaches with different statistical values of the initial geometrical imperfection amplitude $e_0$ are presented, lognormal and normal distributions referred to as the #LN and #G approach, respectively. Correlation between the ultimate resistance of stainless steel columns in compression and input parameters is discussed, with a focus on the influence of $e_0$.

Lognormal distribution of geometric imperfection has also been considered in a study by Chen et al. [41], who analysed concrete-filled steel tubular (CFST) trusses under flexural loading, where the initial steel imperfection amplitude was randomly scaled using Monte-Carlo and LHS methods, based on corresponding statistics. In addition to the steel imperfection, two other concrete imperfections were introduced [41] (binominal to determine its presence and Weibull for the amplitude). In this paper, there is only one geometrical imperfection, which is always present, and in the #LN approach, the values are based on suitable statistic data [40]. The initial imperfection could also be modelled as a linear combination of several scaled buckling modes, as described by Chen et al. [42], where this approach has been utilized for more complex structures with several components (truss structure). In this study, only one buckling mode is utilized to introduce the geometrical imperfection. This is sufficient due to the rather simple geometry of the pin-ended column analysed in this study.

## 2. Determination of the ultimate resistance

### 2.1. Design resistance values of members in flexural buckling

The design process in accordance with Eurocode EN 1993-1-4 [11] was used to determine the design resistance values of the members exposed to flexural buckling under the compressive loading. The design buckling resistance of a compression member $N_{b,Rd}$ for cross-section classes 1–3 is considered as:

$$N_{b,Rd} = \frac{\chi \bullet A \bullet \sigma_{0.2,n}}{\gamma_{M1}} \tag{1}$$

where $\gamma_{M1}$ is a partial factor for resistance of members to instability assessed by member checks (buckling resistance) [11]. The recommended value for stainless steel members $\gamma_{M1} = 1.1$ was used. $A$ is the cross-section area, $\sigma_{0.2,n}$ is the 0.2% proof stress (nominal value), and $\chi$ is the reduction factor for the relevant buckling mode defined as:

$$\chi = min\left\{1.0;\ \frac{1}{\phi + \left[\phi^2 - \bar{\lambda}^2\right]^{0.5}}\right\} \tag{2}$$

where the value of $\phi$ is defined as:

$$\phi = 0.5\left[1 + \alpha\left(\bar{\lambda} - \bar{\lambda}_0\right) + \bar{\lambda}^2\right] \tag{3}$$

where $\alpha$ is an imperfection factor considered as $\alpha = 0.49$, $\bar{\lambda}_0$ is the limiting slenderness with the value $\bar{\lambda}_0 = 0.4$, and $\bar{\lambda}$ is the global slenderness.

In this study, columns exposed to flexural buckling of 15 different global slenderness $\bar{\lambda}$ are analysed. According to EN 1993-1-4 [11], the analysed cross-section CHS 80 × 1.5 is classified as class 1, therefore the global slenderness values $\bar{\lambda}$ are calculated using Eq. (4), which is suitable for cross-sections of classes 1–3 [11]:

$$\bar{\lambda} = \sqrt{\frac{A \bullet \sigma_{0.2,n} \bullet L^2}{\pi^2 \bullet E \bullet I}}, \tag{4}$$

where $\sigma_{0.2,n}$ is the 0.2% proof stress (nominal value), $E$ is elastic Young's modulus, $A$ is the cross-section area and $I$ is the second-moment area of the CHS 80 × 1.5. $L$ is the effective structural length of the column (knife-edge included).

The austenitic stainless steel of material grade EN 1.4307 [43] is considered for the evaluation of the structural resistance (in the product form of a hot rolled plate). Nominal values of this material were considered by Eurocode [11]: the 0.2% proof stress $\sigma_{0.2,n} = 200$ MPa and the ultimate stress as $\sigma_{u,n} = 500$ MPa. Young's modulus value of the considered austenitic steel is $E = 200$ GPa (chapter 2.1.3. from [11]).

The analysed slenderness ratios are summarized in Table 1.

### 2.2. Structural reliability

In order to perform the reliability analysis of the CHS 80 × 1.5 columns loaded axially in compression, the first-order reliability method (FORM) along with a semi-probabilistic approach is adopted. In this approach, only the distribution of the structural resistance is known and is treated as a stochastic variable. A fully probabilistic approach would entail the modelling of the load as a stochastic variable as well. Since random variables are statistically uncorrelated, the resistance can be studied independently of the load.

Reliability design conditions of the European standard EN 1990 [39] are based on the FORM method, which has become one of the most important methods to evaluate structural reliability, especially when combined with the finite element method (FEM), as discussed, e.g., by Faber [44] or Zhao and Ono [45]. The concept of the FORM method is described, e.g., in [46–48]

The expression of the structural reliability is stated as a function of the random load effect $E$ and the random resistance $R$. Safety margin $M$ is defined as:

$$M = R - E \geq 0 \tag{5}$$

The probability of a failure is then expressed as:

$$P_f = P(R < E) = P(R - E < 0) = P(M < 0) \tag{6}$$

It is assumed that $E$, $R$ are statistically independent variables; both with Gauss probability density functions (pdf) with the standard deviations $\sigma_E$, $\sigma_R$ and mean values $\mu_E$, $\mu_R$, respectively. The safety margin $M$ is also in the shape of Gauss pdf defined by standard deviation $\sigma_M$ and mean value $\mu_M$, and is expressed as:

$$\mu_M = \mu_R - \mu_E \tag{7}$$

$$\sigma_M = \sqrt{\sigma_R{}^2 + \sigma_E{}^2} \tag{8}$$

The integration of the probability density function (pdf) of a random variable $M$ expresses the probability of $R - E = M < 0$ as:

$$P_f = \int_{-\infty}^{0} f_M dm = \Phi\left(\frac{0 - \mu_M}{\sigma_M}\right) = \Phi(-\beta) \tag{9}$$

where Φ() is the normalized cumulative Gauss distribution and the ratio $\mu_M/\sigma_M$ is the reliability index $\beta$. The required value of the reliability index of structural members (50 years reference time, safety level of reliability class RC2) according to the standard EN 1990 [39] is $\beta_d = 3.8$, and the probability of failure is then determined as $P_f = \Phi(-3.8) = 7.2 \cdot 10^{-5}$. The reliability is in general verified by the formula:

$$\beta = \frac{\mu_M}{\sigma_M} \geq \beta_d \tag{10}$$

This equation, when substituted into the Eq. (9), represents the condition of the probabilistic design $P_f < P_{fd}$, where $P_{fd}$ is the target value of the failure probability [39]. Eq. (10) can be transformed for feasible practical use by the introduction of the FORM sensitivity factors $\alpha_E$, and $\alpha_R$. These are obtained from the Eq. (8):

$$\sigma_M = \frac{\sigma_R{}^2 + \sigma_E{}^2}{\sqrt{\sigma_R{}^2 + \sigma_E{}^2}} = \frac{\sigma_R}{\sqrt{\sigma_R{}^2 + \sigma_E{}^2}}\sigma_R + \frac{\sigma_E}{\sqrt{\sigma_R{}^2 + \sigma_E{}^2}}\sigma_E \tag{11}$$

$$\sigma_M = \alpha_R\sigma_R + \alpha_E\sigma_E \tag{12}$$

The European standard [39] allows the use of $\alpha_R$ and $\alpha_E$ as constants with values $\alpha_R = 0.8$ and $\alpha_E = 0.7$. For common values of $\sigma_R$ and $\sigma_E$ (conditions of the common design), this simplification leads to $\sigma_M \approx 0.8\ \sigma_R + 0.7\ \sigma_E$. By substituting the Eqs. (7) and (12) into the Eq. (10), the design condition of reliability is obtained as:

$$\mu_E + \alpha_E\beta_d\sigma_E \leq \mu_R - \alpha_R\beta_d\sigma_R, \tag{13}$$

where the left side expresses the design load $E_d$ and the right side the design value of the resistance $R_d$:

$$R_d = \mu_R - 0.8\beta_d\sigma_R \tag{14}$$

The expression for the probability that the structural resistance is lower than the design value is:

$$P(R \leq R_d) = \Phi\left(\frac{\mu_R - \alpha_R\beta_d\sigma_R - \mu_R}{\sigma_R}\right) = \Phi(-\alpha_R\beta_d) \tag{15}$$

In this study, for the FORM sensitivity factor for the resistance $\alpha_R = 0.8$ and the adopted value of the reliability index $\beta = \beta_d = 3.8$, the probability that the structural resistance is lower than the design resistance determined by Eq. (13) is $\Phi(-0.8 \cdot 3.8) = 0.118\%$. This value can be approximately applied as a 0.1% quantile of resistance pdf [49–52]. Therefore, the quantile resistance values discussed in this study are determined by the use of Eq. (13).

## 3. Numerical finite element model

Parametrized numerical finite element models were created utilizing the ANSYS Classic technology (v.20) [38] along with APDL macros. The number of input variable parameters was ten (three geometrical parameters, the amplitude of the initial global geometrical imperfection, and seven material parameters, as described in detail in the following chapters).

### 3.1. Model geometry and boundary conditions

The columns of the circular hollow section (CHS) are considered pin-ended, therefore simply supported, with hinges in one direction at both ends of the columns ($rot_y \neq 0$, see Fig. 1). The cross-section is CHS 80 × 1.5 (the reason for this geometry is explained in chapter 3.4). The parameter $D$ (nominal value of outer tube diameter) is defined by the mean value of 80 mm and the coefficient of variation (CoV) equal to 0.44%. The parameter $t$ (nominal value of tube wall thickness) is considered by the mean value of 1.5 mm, and the CoV of 4.58%. The mean values and CoV of diameter $D$ and the thickness $t$ are considered based on the research by Kala et al. [53]. Fifteen different values of the effective structural length $L$ (additional knife edge lengths included) are considered, to analyse the sufficiently large scale of the slenderness (0.2–1.8). The standard deviation of the structural length is 0.5 mm (considered as half of the smallest part of the regularly used length of measuring devices).

The pin-ended column boundary condition was simulated by

**Table 1**
Structural lengths $L$ of the analysed columns and slenderness ratios.

| $\bar{\lambda}$ [−] | $L$ [m] | $\bar{\lambda}$ [−] | $L$ [m] | $\bar{\lambda}$ [−] | $L$ [m] |
|---|---|---|---|---|---|
| 0.20 | 550 | 0.69 | 1900 | 1.20 | 3300 |
| 0.31 | 850 | 0.80 | 2200 | 1.29 | 3550 |
| 0.40 | 1100 | 0.89 | 2450 | 1.38 | 3800 |
| 0.49 | 1350 | 0.98 | 2700 | 1.60 | 4400 |
| 0.60 | 1650 | 1.09 | 3000 | 1.81 | 5000 |

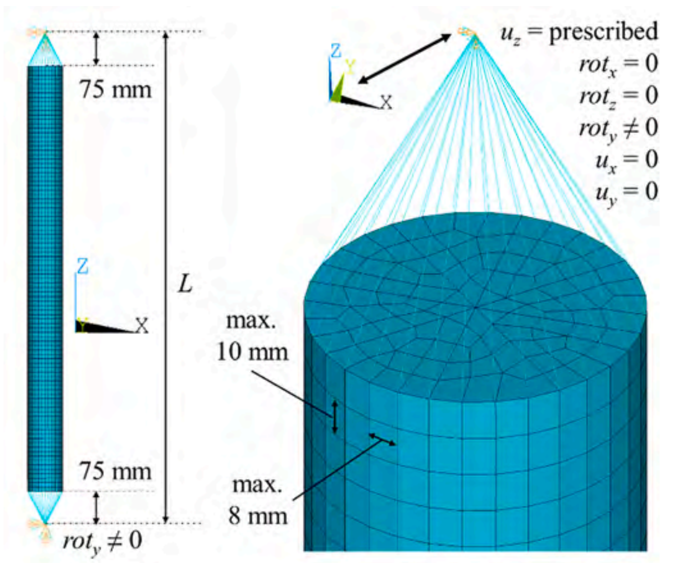


**Fig. 1.** Numerical FEM model of CHS column; mesh geometry.

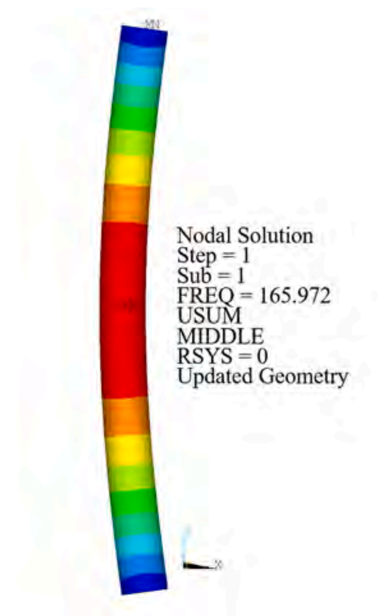


**Fig. 2.** Example of modal analysis results; 1st eigenmode to determine global imperfection.

connecting the circumferential nodes of the CHS tube end in the radial direction with a single node located on the tube longitudinal axis (at both ends). The distance of this node from the cross-sectional plane of the column end is known as the knife-edge length, considered as 75 mm for both ends of the column. These connections between nodes are modelled adopting rather stiff beam elements. For the bottom node, only rotation along the y-axis of the global coordinate system (GCS) is allowed, all other degrees of freedom are constrained. For the upper node, the translation along the z-axis of the GCS (CHS tube axis) is prescribed to provide the loading conducted by a displacement.

Four-node structural shell finite elements (SHELL 181), with six degrees of freedom (DoF) per node (three translational and three rotational), were used for the description of the geometry of the CHS columns numerical model. One integration point in a planar view (three through the element thickness) has been considered (reduced integration), along with the hourglass control feature. The stiffness of these elements consists of membrane and bending parts (Mindlin-Reissner theory), and the transverse shear deformation effect is adopted as linear. Bathe-Dvorkin shear strain formulation is utilized to alleviate shear locking [38].

Geometrically, all the shell elements of the CHS columns along the tube are rectangles, with a maximal edge size of 8 mm along the tube circumference (in the tangential direction) and 10 mm in the longitudinal direction parallel to the z-axis of the GCS (in Fig. 1).

A previous study by Jindra et al. [54] revealed, that FEM analysis using the element formulation described above resulted in a good agreement with the experimental data, and provided a sufficient balance between the accuracy of results and the computational time demand.

### 3.2. Initial geometrical imperfections

The forms of the lowest global buckling modal shapes obtained from the prior modal analyses were utilized to incorporate the initial global geometrical imperfection $e_0$ into the numerical finite element model. The imperfection has the shape of a half-wave sine function with an amplitude $e_0$, see Fig. 2. The $e_0$ limits $L/750$ or $L/1000$ according to the standards [55–57] are independent of the steel grade or type [58].

In this article, two approaches with different distributions of the initial geometrical imperfection amplitudes are used, the lognormal (approach #LN) and normal (Gauss, approach #G).

The approach #G is based on the tolerance limits $\pm L/1000$. The approach #G uses the mean value of the initial geometrical imperfection $e_{0,mean} = 0$, and the standard deviation $e_{0,st.dev} = L/1960$, where 95% of observations of amplitude $e_0$ lie within the tolerance limits $\pm L/1000$, see e.g. [46,48,59,60]. Although these statistics are used for hot-rolled carbon steel members [46,48,59,60], they may not be valid for stainless steel members, see the statistical research by Arrayago et al. [40].

The #LN approach is based on statistical research [40], where a non-zero value of $e_{0,mean} = L/3484$ was utilized along with $e_{0,st.dev} = L/6056$.

The standard deviation of stainless steel members is up to three times lower. This can have a great effect on the design resistance of the columns with intermediate slenderness. Based on statistics [40], it is possible to propose the introduction of a new tolerance limit $L/1666$ for stainless steels, which can replace the classic tolerance limit $L/1000$, see Fig. 3. This article highlights this difference and compares the effect of both approaches on the design resistance using statistical analysis.

The local initial geometrical imperfections were neglected. In comparison to cold-rolled stainless steel sections, hot-formed columns typically have cross-sections with lower values of local slenderness and generally do not fail through the interactions of local and overall buckling modes [61]. The influence of the local geometrical

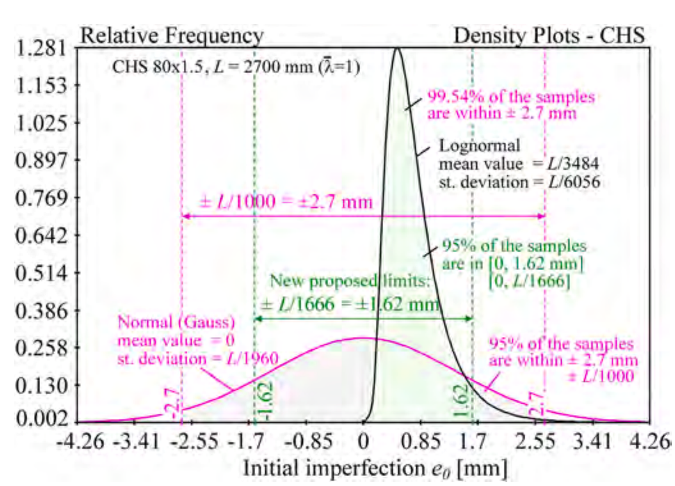


**Fig. 3.** Example of tolerance limits and statistics of approaches #G and #LN for strut with non-dimensional slenderness one.

imperfections is not so significant for the global structural response of the analysed CHS columns [54].

### 3.3. Material model

A stress-strain relation proposed by Ramberg and Osgood [62] is suitable to describe the material behaviour of the austenitic stainless steel. The relation was modified by Hill [63] and was adopted in this study as:

$$\varepsilon = \frac{\sigma}{E_0} + 0.002 \bullet \left(\frac{\sigma}{\sigma_{0.2}}\right)^{n} \tag{16}$$

where $\varepsilon$ and $\sigma$ are engineering strain and stress, respectively, $\sigma_{0.2}$ is the 0.2% proof stress, $E_0$ is the elastic Young's modulus of the material, and $n$ is an exponent parameter to describe the strain-hardening. It was revealed that the stress values above the $\sigma_{0.2}$ are overestimated when using this one-stage material curve [64]. Therefore, a compound two-stage stress-strain relation devised by Mirambell and Real [65] was later adopted, which provided a better agreement with the experimental data for stresses larger than the 0.2% proof stress value. A certain modification of the second stage was proposed by Gardner [26]:

$$\varepsilon = \frac{\sigma - \sigma_{0.2}}{E_{0.2}} + \left(\varepsilon_{tu} - \varepsilon_{t0.2} - \frac{\sigma_u - \sigma_{0.2}}{E_{0.2}}\right) \bullet \left(\frac{\sigma - \sigma_{0.2}}{\sigma_u - \sigma_{0.2}}\right)^{m} + \varepsilon_{t0.2} \Leftrightarrow \sigma > \sigma_{0.2} \tag{17}$$

where $\sigma_u$ is the ultimate stress of the stainless steel material, $\varepsilon_{tu}$ is the total strain at the ultimate stress, $\varepsilon_{t0.2}$ is the total strain at the 0.2% proof stress, $m$ is an exponent parameter to describe the strain hardening above the $\sigma_{0.2}$ value, and $E_{0.2}$ is the tangent modulus (stiffness) at the $\sigma_{0.2}$ stress defined as:

$$E_{0.2} = \frac{E_0}{1 + 0.002 \bullet n \bullet \frac{E_0}{\sigma_{0.2}}} \tag{18}$$

The multilinear material model with isotropic hardening (Von Mises plasticity yield surface criterion) was adopted during the numerical analyses. The analytical material curve is discretized considering a sufficiently small step in order to utilize the multilinear description. A more detailed description of this material model implementation process is described in the author's previous study [66]. The transfer from the nominal (engineering) stress-strain material curves into the true (logarithmic) stress-strain material dependences were considered to be in match with the process of the geometrically nonlinear analysis [38]:

$$\sigma_{true} = \sigma_{nom} \bullet (1 + \varepsilon_{nom}) \tag{19}$$

$$\varepsilon_{true} = ln(1 + \varepsilon_{nom}) \tag{20}$$

where $\sigma_{nom}$ and $\varepsilon_{nom}$ are nominal (engineering) stress and strain respectively, $\sigma_{true}$ is the true stress and $\varepsilon_{true}$ is the true total (mechanical) strain. Values of the $\varepsilon_{nom}$ were introduced with the negative sign for the compressive material properties, which results in a negative tangent of the stress-strain material curve from a certain point. Such a definition is however not feasible utilizing the isotropic hardening [38]. Therefore, the definition of ideal plasticity (small positive tangent practically close to 0.0) was used after the point of the peak stress (Fig. 4).

The maximum sensitivity of ultimate resistance to the residual stress occurs for the non-dimensional slenderness of 0.8 in the case of flexural buckling of a hot-rolled member with cross-section IPN 200 [60]. The maximum sensitivity to initial geometric imperfection occurs for non-dimensional-slenderness of 1.1 [60]. The sensitivity to the residual stress and initial geometric imperfection is low for very short or very slender columns, independent of the cross-section. The absolute effect on resistance is given by the magnitude of the residual stress and redistribution across the cross-section during stressing. Not very significant values of the membrane residual stresses were observed in hot rolled CHS members, therefore it is possible to neglect these stresses [67]. Besides initial geometric imperfection, welding residual stress and deformation can also affect the column resistance, which might be crucial for intermediate slenderness (non-dimensional slenderness around 1.0). The resistance of very slender columns is less sensitive to these influences, because the stress at the load level, which is equal to the ultimate resistance, is relatively small. Through-thickness residual stresses are implicitly incorporated by considering the measured values of the material properties [68] (in this study values based on statistical data) or indirectly incorporated by initial geometrical imperfections [40]. The mean values and CoV of the material parameters utilized in this study are based on the comprehensive statistical study by Arrayago et al. [40]. The parameter values are based on the corresponding tables from this study for the austenitic stainless steel material.

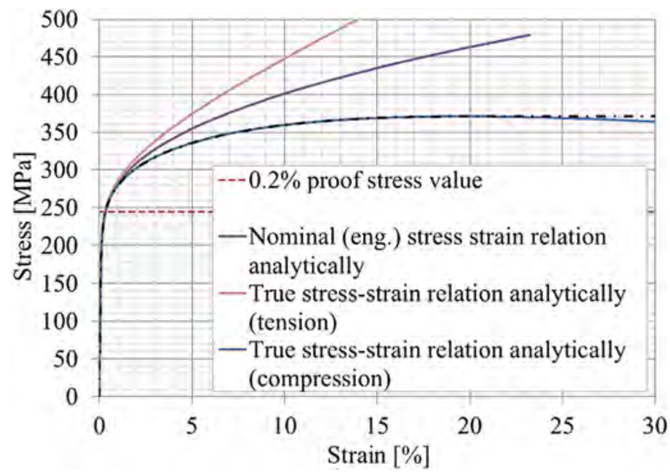


**Fig. 4.** Material model verification by one element uniaxial tests.

### 3.4. Numerical model validation

The numerical finite element model of the CHS column in flexural buckling analysed in this study was previously validated in a study by Jindra et al. [54]. Data from a comprehensive experimental program conducted at Imperial College London (ILC) and Universitat Politècnica de Catalunya (UPC) have been obtained from a study by Buchanan et al. [34]. The physical experiments included 37 various stainless steel columns subjected to flexural buckling. The specimens differed in structural length, material grades, and cross-sectional dimensions. Five different CHS cross-sections have been experimentally analysed and are well documented by Buchanan et al. [34]: 80 × 1.5, 88.9 × 2.6, 101.6 × 1.5, 104 × 2, and 106 × 3. In this study, one of the CHS geometries previously utilized for the numerical model validation [54] was considered for the subsequent reliability analysis presented in this paper. CHS 80 × 1.5 was preferred due to its smallest cross-sectional area, resulting in shorter columns (for each of the fifteen considered slenderness values) compared to CHS of larger geometries. Therefore, fewer finite elements were considered for the adopted mesh size resulting in savings in the computational time of each random realization. This is generally more effective when a large number of numerical analyses need to be conducted.

In both studies [34,54], two sets of material property values (noted as TP - based on tensile properties, and SCP – based on the stub column properties) were considered, which is explained in more detail in the study by Buchanan et al. [54], and the numerical models are validated for each of these sets of material parameters separately in both studies [34,54]. Both validations are conducted utilizing the mean (averaged) value of the normalized ultimate resistances, which is determined as:

$$N_{u,norm,AM} = \frac{1}{37}\sum_{i=1}^{37}\left(\frac{N_{u,FE,i}}{N_{u,exp,i}}\right) \tag{21}$$

where $N_{u,exp,i}$ is the ultimate resistance based on the physical i-th experiment, $N_{u,FE,i}$ is the ultimate resistance obtained from the corresponding i-th numerical FEM simulation, and the number 37 indicates the total number of conducted experiments. The average value of the normalized ultimate resistance along with the standard deviation bars of the normalized resistances set utilizing the SCP material properties are graphically depicted in Fig. 5. The performance of the TP material properties had only a slightly higher standard deviation [34,54]. The average value of the normalized ultimate resistance is 0.998 (standard deviation 0.050) in the validation study [54] and 1.013 (standard deviation 0.047) in the study by Buchanan et al. [34]. These normalized values are very close to 1, with rather small values of the standard deviation. This indicates, that a very good agreement between the physical experiments and numerical simulations was achieved. Therefore, the numerical FEM models might be considered as properly validated [54] and suitable for the reliability analysis presented in this paper.

## 4. FEM simulations and statistic verification

### 4.1. Statistical parameters

The statistical information about the material and geometric parameter values of the analysed CHS columns is required to conduct a reliability analysis utilizing GMNIA (geometrically and materially nonlinear analyses with imperfections).

All the required statistics for material parameters were based on the comprehensive statistical study by Arrayago et al. [40], as well as the initial imperfection amplitude $e_0$ for the #LN approach. The statistics for geometrical parameters were based on a study by Kala et al. [53]. In the #G modelling approach, it is assumed that 95% of the random imperfection realizations are within the tolerance limits of $\pm L/1000$. The standard deviation of the initial geometrical imperfection $\sigma_e$ under this assumption results in $L/1960$, see e.g., Jönsson et al. [46]. The mean values along with the standard deviations of all the input parameters are summarized in Table 2, as well as the utilized distribution type of the parameter's pdf. The mutual dependence between material parameters is adopted in accordance with the correlation matrix provided by Arrayago et al. [40]. The correlations between material and all other parameters, geometrical parameters $D$, $t$, $L$, and the initial geometrical imperfection $e_0$, are neglected. Also, these remaining parameters are considered as mutually statistically independent. An example of a correlation matrix of all the input parameters is provided in Fig. 6.

For the stainless steel material, the Poisson ratio is used as constant $\nu = 0.3$. This constant is assumed analogically to the standard carbon steel material in accordance with the results of a stochastic sensitivity analysis by Kala [69].

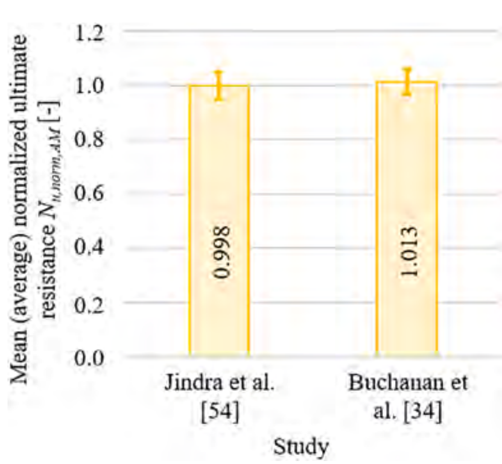


**Fig. 5.** Numerical FEM model validation.

### 4.2. Numerical FEM simulations

Numerical finite element simulations are performed for all the 15 different flexural buckling relative slenderness ratios $\overline{\lambda}$ (Table 1), each with 200 samples of the CHS columns.

These 200 random realizations of the 10 random inputs (6 material parameters, 3 geometric, and the initial imperfection $e_0$) were generated using the Advanced Latin Hypercube Sampling (ALHS) method. Utilizing ALHS, the correlation errors are minimized by the strategies of stochastic evolution [70]. In the standard Latin Hypercube Sampling (LHS) method [71], the representation of the input distributions and the specified input correlations is also very accurate, and the minimization of undesired correlations is performed utilizing the method in accordance with Iman and Conover [72]. For a smaller number of input variables, ALHS is recommended [73]. Software OptiSLang [73] was used to manage the ALHS sampling and communication with the ANSYS solver.

Each numerical simulation was conducted using both approaches of distribution type (#G and #LN) of the initial geometrical imperfection $e_0$. This corresponds with $15 \cdot 2 \cdot 200 = 6000$ numerical simulations in total. For each of the 15 slenderness values of each $e_0$ modelling approach (#LN, #G), brand new values for all 200 random realizations of each input parameter were generated.

The ultimate compressive force $N_u$ was obtained for every single simulation in order to create the database for the subsequent probabilistic determination of the 0.1% quantile. The ultimate compressive force $N_u$ of each numerical simulation is considered as the maximal value of the force-displacement curve. An example of force-displacement curves is provided also in Fig. 7. In this example, the curve marked as the "mean value" of the force-displacement curves is determined by techniques of averaging the corresponding values of the function range $f(u_x)$ for the values of the function domains $u_x$ [73]. The maximum of the "averaged curve" is not considered for further processing.

### 4.3. Statistic verification

The Gaussian distribution of the results was verified to check the statistical validity of the results. This was conducted by testing the data from each relative slenderness value for each approach (#G and #LN) separately. The Chi-square distribution test or the so-called "goodness-of-fit" test [74] was utilized to confirm the assumption that the considered population sample has a certain probability distribution. The testing result revealed that the hypothesis of Gauss distribution of the results (1% significance level) was not rejected. The test was also conducted with the shifted lognormal and Hermite distributions. The Chi-square distribution testing concluded that the ultimate resistance results obtained from the numerical finite element simulations can be considered as normally distributed in all slenderness cases. In most (but not all) cases, Hermite or shifted lognormal distributions could be feasibly adopted in accordance with the conducted "goodness-of-fit" test.

## 5. Reliability analysis

The ability of a structure or a structural member to fulfil the specified requirements during the whole design working life of this member is known as reliability, as described by EC 0 [39]. Regarding the ultimate limit state, the reliability could be interpreted as the ability to withstand the load effects of the member.

In accordance with B.3.2(2) of annex B from the EN 1990 [39], the

**Table 2**
Statistical geometric and material parameters.

| Approach | Parameter | | Unit | Mean value | St. dev. | Distribution type |
|---|---|---|---|---|---|---|
| #G, #LN | Diameter | $D$ | [mm] | 80 | 0.3538 | Normal |
| #G, #LN | Thickness | $t$ | [mm] | 1.5 | 0.0687 | Normal |
| #G, #LN | Structural length | $L$ | [mm] | various | 0.5 | Normal |
| #G, #LN | Young's Elastic modulus | $E$ | [GPa] | 195.416 | 11.175 | Normal |
| #G, #LN | Exponent parameter | $m$ | [−] | 2.3 | 0.3 | Lognormal |
| #G, #LN | Exponent parameter | $n$ | [−] | 10.6 | 1.8 | Lognormal |
| #G, #LN | Ultimate strain | $\varepsilon_u$ | [−] | 0.49 | 0.06 | Normal |
| #G, #LN | Ultimate stress | $\sigma_u$ | [MPa] | 575 | 20 | Lognormal |
| #G, #LN | 0.2% proof (yield) stress | $\sigma_{0.2}$ | [MPa] | 244 | 15 | Lognormal |
| #G | Initial imperfection | $e_0$ | [mm] | 0 | $L$/1960 | Normal |
| #LN | Initial imperfection | $e_0$ | [mm] | $L$/3484 | $L$/6056 | Lognormal |

| | $D$ | $e_0$ | $E$ | $L$ | $t$ | $\sigma_u$ | $\varepsilon_u$ | $\sigma_{0.2}$ | $m$ | $n$ |
|---|---|---|---|---|---|---|---|---|---|---|
| $D$ | 1.00 | 0.01 | 0.01 | 0.03 | 0.01 | 0.02 | -0.06 | 0.04 | 0.04 | 0.01 |
| $e_0$ | 0.01 | 1.00 | -0.01 | 0.05 | 0.04 | -0.02 | 0.06 | -0.04 | -0.03 | -0.03 |
| $E$ | 0.01 | -0.01 | 1.00 | -0.05 | -0.02 | -0.11 | 0.30 | -0.16 | -0.20 | 0.03 |
| $L$ | 0.03 | 0.05 | -0.05 | 1.00 | -0.04 | -0.02 | 0.00 | -0.01 | -0.01 | 0.05 |
| $t$ | 0.01 | 0.04 | -0.02 | -0.04 | 1.00 | 0.01 | 0.01 | -0.01 | 0.01 | -0.02 |
| $\sigma_u$ | 0.02 | -0.02 | -0.11 | -0.02 | 0.01 | 1.00 | -0.51 | 0.80 | 0.36 | -0.32 |
| $\varepsilon_u$ | -0.06 | 0.06 | 0.30 | 0.00 | 0.01 | -0.51 | 1.00 | -0.75 | -0.43 | 0.16 |
| $\sigma_{0.2}$ | 0.04 | -0.04 | -0.16 | -0.01 | -0.01 | 0.80 | -0.75 | 1.00 | 0.47 | -0.33 |
| $m$ | 0.04 | -0.03 | -0.20 | -0.01 | 0.01 | 0.36 | -0.43 | 0.47 | 1.00 | -0.29 |
| $n$ | 0.01 | -0.03 | 0.03 | 0.05 | -0.02 | -0.32 | 0.16 | -0.33 | -0.29 | 1.00 |

**Fig. 6.** Example of correlation matrix of all the input parameters, slenderness 1.0, #LN.

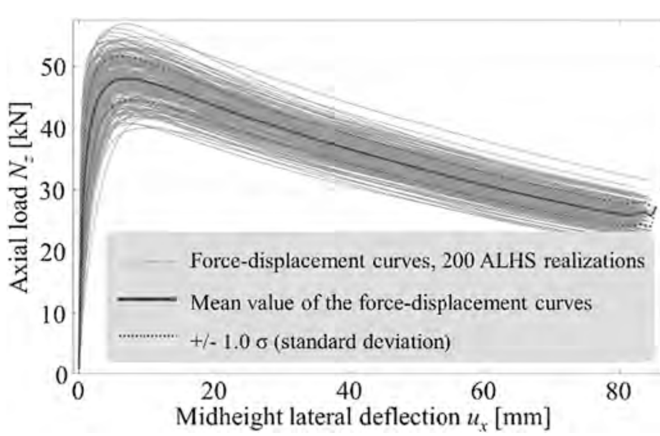


**Fig. 7.** Example of Load vs. midheight lateral deflection curves, slenderness 1.1, #LN.

reliability classes RC1-RC3 may be associated with the consequence classes CC1-CC3, respectively. For the RC2 (corresponds with the CC2) and 50 year reference period, table B2 [39] recommends a minimal value of the reliability index $\beta_d = 3.8$. Chapter C.7(3) of annex C of EN 1990 [39] then allows consideration of the FORM sensitivity factor for the resistance as $\alpha_R = 0.8$. The probability that the resistance would be lower than the design value is:

$$\Phi(-\alpha_R\beta_d) = \Phi(-0.8\bullet 3.8) = 0.1183\% \tag{22}$$

The value corresponds approximately with the 0.1% quantile of the resistance distribution and is applicable for the comparison of the results between the reliability analysis and the resistances calculated in accordance with the EC 3 [11] (also described in chapter 2.1 of this paper). For each data set, the resistance simulation database, the standard deviation $\sigma_R$, and the mean value $\mu_R$ of the 200 realizations are used to determine the 0.1% resistance quantile $R_{0.1\%}$, defined as:

$$R_{0.1\%} = \mu_R - \alpha_R\beta_d\sigma_R = \mu_R - 0.8\bullet 3.8\bullet \sigma_R \tag{23}$$

## 6. Results

The results of all the numerical simulations (ultimate compressive forces $N_u$) in the form of statistical parameters (standard deviation, mean value, 0.1% quantiles, etc.) are summarized in Table 3 and Table 4 for modelling approaches #LN and #G respectively. For several slenderness values, the standard skewness resulted in negative values. Therefore, the shifted lognormal distribution (along with the corresponding 0.1% quantile of the pdf) is not applicable for these cases. The values in the "EC 0" columns of these tables are obtained utilizing Eq. (14) (analogically Eq. (23)), and the values in the "EC 3" columns are calculated using Eq. (1) (chapter 2.1 of this paper).

The standard skewness and standard kurtosis show a relatively high statistical error due to a relatively small number of ALHS simulations (200 runs). This is reflected also in the 0.1% quantile estimations for the Shifted lognormal and Hermite distributions. Consequently, the conclusions are made using only Gauss pdf along with the 0.1% quantile of Gauss distribution.

The graphical comparison of the GMNIA FORM results with the continuous flexural buckling curve in accordance with the EC 3 design approach is depicted in Fig. 8. Additionally, the flexural buckling curve in accordance with the EC 3 considering the design provisions proposed by Buchanan et al. [34] is plotted. The only difference between these two flexural buckling curves is in the adoption of a different limit slenderness value $\overline{\lambda}_0$. For the "EC 3" curve, this value is considered as 0.4 [11], and for the "EC 3 + Buchanan" curve as 0.2 [34]. The value is used in Eq. (3) (see chapter 2.1).

The Pearson (linear) correlation between $N_u$ and $e_0$ was investigated, and the values are graphically depicted in Fig. 9 and Fig. 10 for the $e_0$ modelling approaches #LN and #G respectively.

Some specific aspects of modelling can be commented on in more detail. As a consequence of the zero mean value of the initial global geometrical imperfection $e_0$ (modelling approach #G), few random realizations of $e_0$ resulted in very small values of $e_0$, essentially 0. Load-deflection curves for 3 of these cases (of slenderness 0.2, 0.3, and 1.1) are depicted in Fig. 11. Horizontal displacements (in global x-direction) of the slenderness 0.3 are graphically depicted in Fig. 12 in 3 different points (#A0, #A1, and #A2). Point #A0 is the point with the maximal value of the mid-height lateral deflection $u_x$ in the direction opposite to the direction of the introduced initial global geometrical imperfection $e_0$. Hence the minus value in the graph (Fig. 11), even though according to the GCS the displacement is positive (Fig. 12). The introduced

**Table 3**
Results of the ultimate resistance $N_u$ (kN), approach #LN (lognormal pdf of the $e_0$).

| $\overline{\lambda}$ [−] | Mean value | Standard deviation | Standard skewness | Standard kurtosis | 0.1% quantile Hermite | Shifted lognormal | normal | EC 0 (FORM) formula | EC 3 design value | EC 3 + Buchanan et al. [34] |
|---|---|---|---|---|---|---|---|---|---|---|
| 0.20 | 93.91 | 8.46 | 0.42 | 3.29 | 70.30 | 72.36 | 67.75 | 68.18 | 67.26 | 67.26 |
| 0.31 | 84.17 | 6.60 | 0.10 | 2.51 | 67.70 | 64.73 | 63.77 | 64.10 | 67.26 | 63.56 |
| 0.40 | 78.72 | 5.95 | 0.31 | 2.81 | 63.29 | 62.83 | 60.34 | 60.64 | 67.26 | 60.39 |
| 0.49 | 74.26 | 5.36 | 0.06 | 2.86 | 58.50 | 58.17 | 57.68 | 57.95 | 63.65 | 57.09 |
| 0.60 | 69.58 | 4.98 | 0.12 | 3.15 | 54.16 | 55.01 | 54.19 | 54.44 | 58.92 | 52.89 |
| 0.69 | 65.92 | 4.70 | 0.39 | 3.62 | 51.51 | 53.80 | 51.40 | 51.64 | 54.66 | 49.20 |
| 0.80 | 61.56 | 4.46 | 0.16 | 3.72 | 46.30 | 48.78 | 47.79 | 48.01 | 49.27 | 44.63 |
| 0.89 | 57.75 | 4.22 | 0.20 | 3.09 | 45.37 | 45.88 | 44.73 | 44.94 | 44.73 | 40.82 |
| 0.98 | 53.62 | 3.75 | 0.07 | 2.60 | 43.56 | 42.38 | 42.02 | 42.21 | 40.34 | 37.14 |
| 1.09 | 48.30 | 3.47 | −0.05 | 2.44 | 38.57 | # | 37.57 | 37.74 | 35.47 | 33.01 |
| 1.20 | 42.75 | 3.08 | −0.10 | 2.92 | 32.82 | # | 33.23 | 33.38 | 31.15 | 29.28 |
| 1.29 | 38.30 | 2.79 | −0.16 | 2.89 | 29.12 | # | 29.68 | 29.82 | 28.00 | 26.52 |
| 1.38 | 34.22 | 2.43 | 0.02 | 2.62 | 27.49 | 26.79 | 26.72 | 26.85 | 25.23 | 24.05 |
| 1.60 | 26.34 | 1.90 | 0.04 | 2.79 | 20.81 | 20.57 | 20.46 | 20.55 | 19.91 | 19.20 |
| 1.81 | 20.71 | 1.52 | −0.01 | 2.82 | 16.13 | # | 16.00 | 16.08 | 16.03 | 15.58 |

**Table 4**
Results of the ultimate resistance $N_u$ (kN), approach #G (normal pdf of the $e_0$).

| $\overline{\lambda}$ [−] | Mean value | Standard deviation | Standard skewness | Standard kurtosis | 0.1% quantile Hermite | Shifted lognormal | normal | EC 0 (FORM) formula | EC 3 design value | EC 3 + Buchanan et al. [34] |
|---|---|---|---|---|---|---|---|---|---|---|
| 0.20 | 93.64 | 8.43 | −0.02 | 2.81 | 68.26 | # | 67.59 | 68.01 | 67.26 | 67.26 |
| 0.31 | 83.85 | 6.70 | 0.20 | 3.07 | 64.33 | 64.97 | 63.16 | 63.49 | 67.26 | 63.56 |
| 0.40 | 78.32 | 5.77 | −0.04 | 2.45 | 62.43 | # | 60.49 | 60.78 | 67.26 | 60.39 |
| 0.49 | 73.92 | 5.69 | 0.21 | 2.88 | 58.09 | 57.93 | 56.33 | 56.61 | 63.65 | 57.09 |
| 0.60 | 69.02 | 4.93 | 0.02 | 3.32 | 52.53 | 53.96 | 53.80 | 54.05 | 58.92 | 52.89 |
| 0.69 | 65.49 | 5.76 | 1.29 | 9.28 | 40.57 | 55.29 | 47.70 | 47.99 | 54.66 | 49.20 |
| 0.80 | 60.60 | 5.02 | 0.18 | 2.54 | 48.60 | 46.36 | 45.09 | 45.35 | 49.27 | 44.63 |
| 0.89 | 56.9 | 4.65 | 0.14 | 3.12 | 42.76 | 43.45 | 42.53 | 42.77 | 44.73 | 40.82 |
| 0.98 | 52.76 | 4.45 | 0.15 | 2.57 | 41.57 | 39.92 | 39.00 | 39.22 | 40.34 | 37.14 |
| 1.09 | 47.48 | 4.27 | 0.13 | 2.43 | 38.55 | 35.07 | 34.29 | 34.50 | 35.47 | 33.01 |
| 1.20 | 42.00 | 3.91 | 0.15 | 2.58 | 32.15 | 30.76 | 29.93 | 30.13 | 31.15 | 29.28 |
| 1.29 | 37.63 | 3.23 | 0.07 | 2.83 | 28.27 | 27.97 | 27.64 | 27.80 | 28.00 | 26.52 |
| 1.38 | 33.68 | 2.99 | −0.09 | 3.33 | 23.23 | # | 24.45 | 24.60 | 25.23 | 24.05 |
| 1.60 | 25.96 | 2.04 | 0.04 | 2.69 | 20.19 | 19.75 | 19.65 | 19.75 | 19.91 | 19.20 |
| 1.81 | 20.46 | 1.66 | 0.17 | 2.46 | 16.89 | 15.72 | 15.34 | 15.42 | 16.03 | 15.58 |

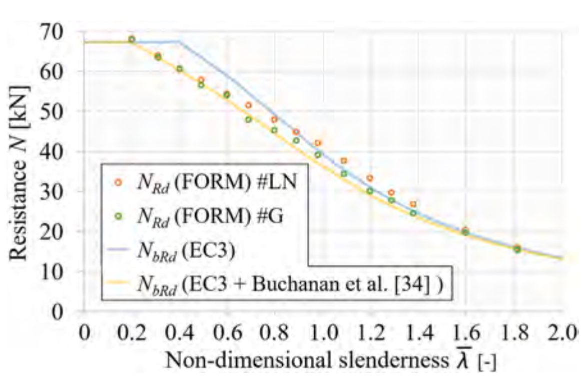


**Fig. 8.** Graphical comparison of the design resistances, FORM vs. EC 3 buckling curve.

direction of the $e_0$ is opposite to the x-axis of the GCS, as indicated by the black arrow in Fig. 12. Points #A1 and #A2 are the global maximum of the curve (ultimate resistance $N_u$) and the last sub-step of the analysis respectively. Points #B1, #B2, #C1 and #C2 are marked analogically (Fig. 11). Equivalent plastic strains (Von Mises) of the CHS members in these selected points are depicted in Fig. 13 for the slenderness 0.3 (#A1, #A2), Fig. 14 for the slenderness 0.2 (#B1, #B2) and in Fig. 15 for the slenderness 1.1 (#C1, #C2).

For all cases, the scale for equivalent plastic strains was fixed (for better comparison) in the interval 0 to 0.25 (25%), with the dark blue colour for plastic strains up to 0.002 (0.2% indicating the equivalent of the yield point of the stainless steel). The smallest and largest values achieved on a specific model are listed above the SMN or SMX scale. The grey area (Fig. 14 #B2, for example) represents the zones where the upper fixed limit was exceeded.

The load-deflection curves of two selected cases from all the realizations of modelling approach #LN are depicted in Fig. 16. The global maximum of the case with the minimal ultimate resistance $N_u$ from the random realizations of the slenderness 0.3 is described as point #D1, and the last converged sub-step as #D2 and the equivalent plastic strains of these points are depicted in Fig. 17. Analogically, Fig. 18 depicts the equivalent plastic strain in points #E1 and #E2 (global maximum and last sub-step) of the random realization of slenderness 1.2 which resulted in the highest ultimate resistance value $N_u$.

## 7. Discussion

### *7.1. General applicability of the considered CHS cross-section dimension*

In this study, one specific geometry of the CHS cross-section, CHS 80 × 1.5 has been utilized to conduct the reliability analysis. It is assumed that the modelling and the analysis results are also applicable for a wider range of CHS geometries. It is however presumed, that for the larger thickness of the CHS tube, the coefficient of variation will be slightly smaller, as it should be easier to fulfil the tolerance range of the

| $\bar{\lambda}$ | | 0.20 | 0.31 | 0.40 | 0.49 | 0.60 | 0.69 | 0.80 | 0.89 | 0.98 | 1.09 | 1.20 | 1.29 | 1.38 | 1.60 | 1.81 |
|---|---|---|---|---|---|---|---|---|---|---|---|---|---|---|---|---|
| correlation $N_u$ vs. | $D$ | 0.06 | 0.12 | 0.11 | 0.06 | 0.11 | 0.03 | 0.12 | 0.11 | 0.15 | 0.12 | 0.15 | 0.17 | 0.21 | 0.23 | 0.13 |
| | $e_0$ | -0.03 | -0.07 | -0.11 | -0.17 | -0.22 | -0.21 | -0.31 | -0.40 | -0.43 | -0.45 | -0.48 | -0.41 | -0.43 | -0.33 | -0.31 |
| | $E$ | -0.13 | -0.13 | -0.04 | 0.03 | -0.04 | -0.02 | 0.11 | 0.19 | 0.19 | 0.33 | 0.48 | 0.57 | 0.62 | 0.67 | 0.74 |
| | $L$ | 0.06 | -0.04 | -0.02 | 0.00 | -0.08 | -0.02 | 0.00 | 0.03 | -0.04 | 0.01 | 0.03 | -0.02 | 0.04 | 0.03 | -0.03 |
| | $t$ | 0.47 | 0.56 | 0.60 | 0.62 | 0.64 | 0.62 | 0.63 | 0.63 | 0.60 | 0.63 | 0.63 | 0.63 | 0.57 | 0.59 | 0.59 |
| | $\sigma_u$ | 0.68 | 0.66 | 0.62 | 0.56 | 0.54 | 0.49 | 0.42 | 0.27 | 0.27 | 0.14 | 0.04 | 0.01 | 0.01 | -0.03 | -0.06 |
| | $\varepsilon_u$ | -0.62 | -0.61 | -0.60 | -0.57 | -0.53 | -0.54 | -0.50 | -0.37 | -0.29 | -0.20 | 0.02 | 0.03 | 0.06 | 0.10 | 0.13 |
| | $\sigma_{0.2}$ | 0.82 | 0.81 | 0.79 | 0.75 | 0.69 | 0.65 | 0.60 | 0.43 | 0.37 | 0.25 | 0.06 | 0.04 | 0.04 | -0.01 | -0.03 |
| | $m$ | 0.61 | 0.41 | 0.37 | 0.31 | 0.26 | 0.30 | 0.25 | 0.12 | 0.09 | 0.06 | -0.12 | -0.05 | -0.02 | -0.04 | -0.13 |
| | $n$ | -0.44 | -0.33 | -0.23 | -0.11 | 0.02 | 0.07 | 0.14 | 0.33 | 0.30 | 0.29 | 0.24 | 0.20 | 0.12 | 0.08 | 0.07 |

**Fig. 9.** Linear correlation between $N_u$ and all 10 input parameters for different slenderness (#LN).

| $\bar{\lambda}$ | | 0.20 | 0.31 | 0.40 | 0.49 | 0.60 | 0.69 | 0.80 | 0.89 | 0.98 | 1.09 | 1.20 | 1.29 | 1.38 | 1.60 | 1.81 |
|---|---|---|---|---|---|---|---|---|---|---|---|---|---|---|---|---|
| correlation $N_u$ vs. | $D$ | 0.07 | 0.06 | 0.08 | 0.09 | 0.04 | 0.07 | 0.02 | 0.07 | 0.03 | 0.12 | 0.04 | 0.11 | 0.06 | 0.16 | 0.18 |
| | $\|e_0\|$ | -0.24 | -0.11 | -0.27 | -0.32 | -0.32 | -0.50 | -0.60 | -0.61 | -0.67 | -0.72 | -0.70 | -0.66 | -0.67 | -0.53 | -0.51 |
| | $E$ | -0.10 | -0.13 | -0.09 | -0.03 | -0.02 | -0.02 | -0.01 | 0.15 | 0.18 | 0.25 | 0.36 | 0.40 | 0.57 | 0.61 | 0.65 |
| | $L$ | 0.00 | 0.00 | 0.06 | -0.03 | -0.10 | -0.10 | -0.04 | -0.11 | 0.07 | -0.11 | -0.06 | 0.06 | 0.01 | 0.01 | -0.01 |
| | $t$ | 0.51 | 0.58 | 0.57 | 0.57 | 0.60 | 0.44 | 0.50 | 0.53 | 0.55 | 0.53 | 0.55 | 0.53 | 0.53 | 0.48 | 0.56 |
| | $\sigma_u$ | 0.62 | 0.59 | 0.60 | 0.55 | 0.51 | 0.49 | 0.44 | 0.35 | 0.22 | 0.06 | 0.12 | 0.06 | 0.06 | -0.04 | -0.09 |
| | $\varepsilon_u$ | -0.65 | -0.59 | -0.54 | -0.53 | -0.50 | -0.43 | -0.44 | -0.31 | -0.21 | -0.09 | -0.12 | 0.02 | 0.02 | 0.13 | 0.08 |
| | $\sigma_{0.2}$ | 0.81 | 0.78 | 0.74 | 0.71 | 0.64 | 0.59 | 0.57 | 0.44 | 0.32 | 0.12 | 0.17 | 0.07 | 0.08 | -0.02 | -0.03 |
| | $m$ | 0.58 | 0.48 | 0.32 | 0.29 | 0.30 | 0.30 | 0.16 | 0.15 | 0.18 | 0.00 | 0.01 | -0.14 | -0.11 | -0.09 | -0.02 |
| | $n$ | -0.36 | -0.40 | -0.25 | -0.08 | -0.04 | 0.07 | 0.20 | 0.16 | 0.16 | 0.30 | 0.16 | 0.14 | 0.14 | 0.13 | 0.15 |

**Fig. 10.** Linear correlation between $N_u$ and all 10 input parameters for different slenderness (#G).

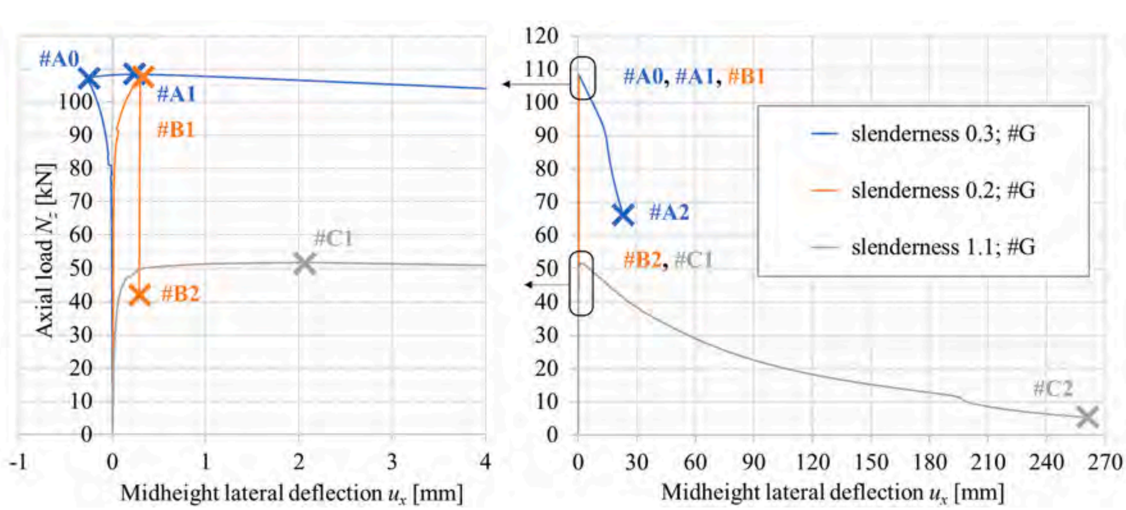


**Fig. 11.** Load-deflection curves of chosen cases with very small initial $e_0$ realization (#G).

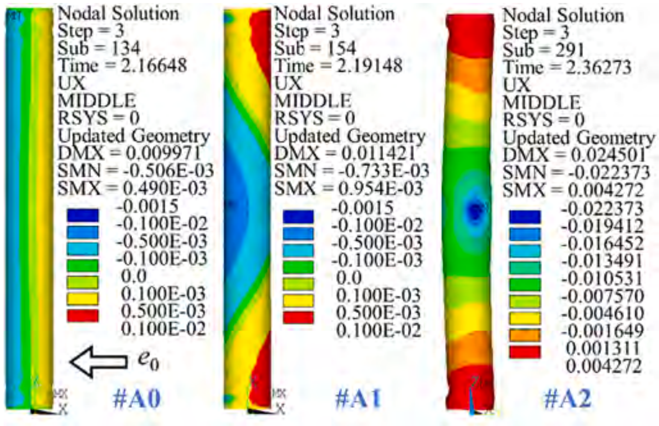


**Fig. 12.** Horizontal displacements of column with very small initial $e_0$ realization (#G), slenderness 0.3.

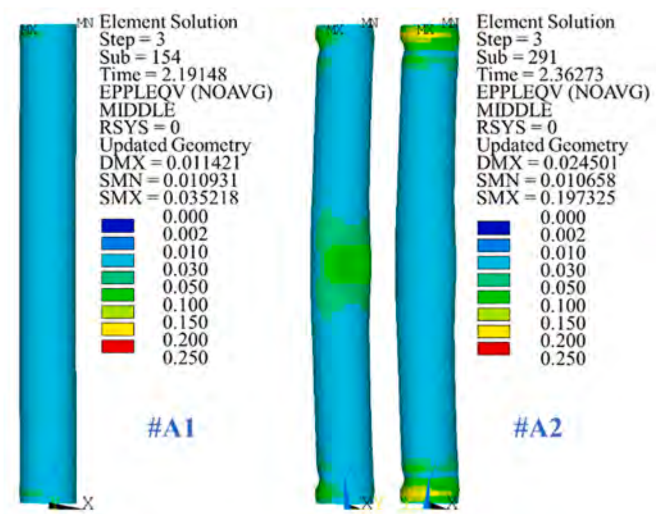


**Fig. 13.** Equivalent plastic strain of column with very small initial $e_0$ realization (#G), slenderness 0.3.

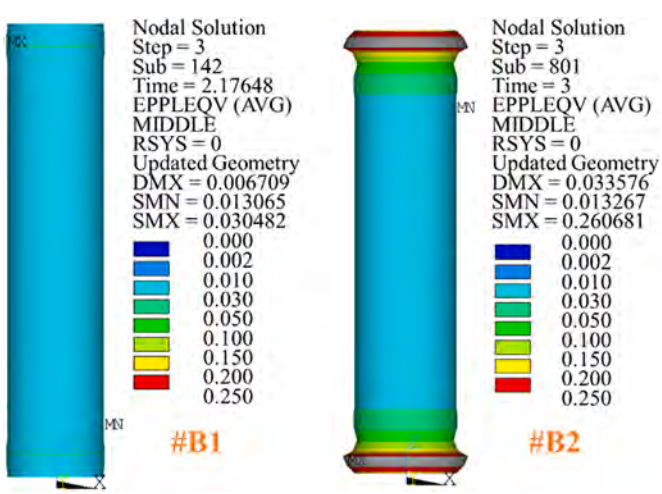


**Fig. 14.** Equivalent plastic strain of column with very small initial $e_0$ realization (#G), slenderness 0.2.

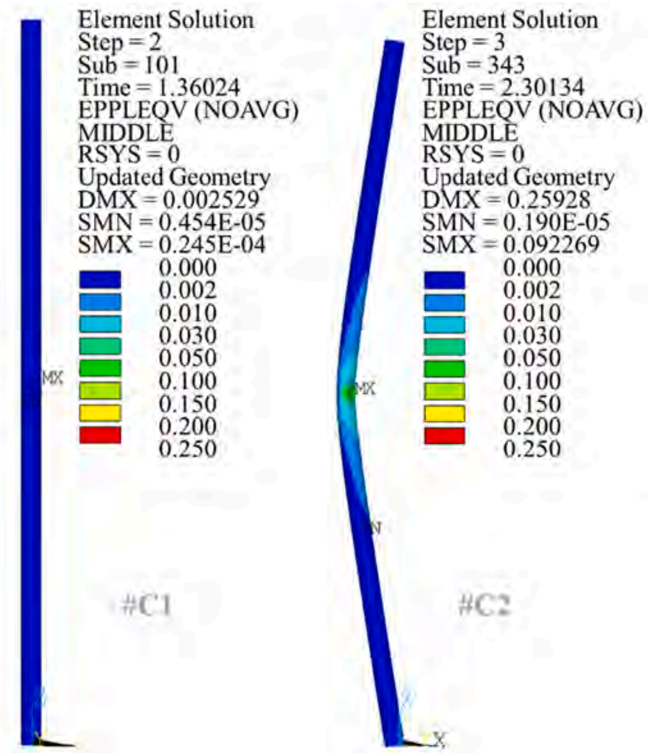


**Fig. 15.** Equivalent plastic strain of column with very small initial $e_0$ realization (#G), slenderness 1.1.

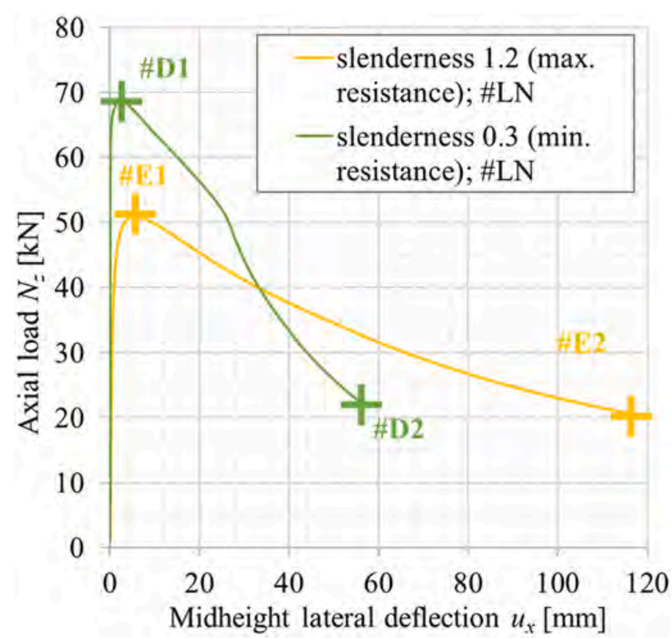


**Fig. 16.** Load-deflection curves of chosen cases (#LN).

thickness if a larger value is manufactured. It is assumed that the influence of different variation coefficients of the CHS thickness would be rather negligible on the global response. Thicker profiles, however, might have other manufacturing imperfections (geometric, or material), which might be worth considering during the analysis process. It is assumed that the modelling approach and the results are applicable for the most commonly used CHS profiles.

This assumption might also be discussed based on the results

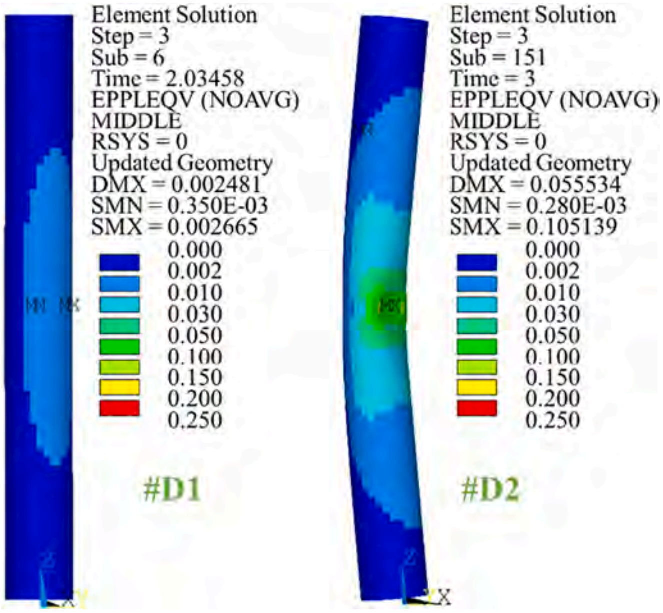


**Fig. 17.** Equivalent plastic strain of column of realization (#LN) with the smallest $N_u$ value from the group of slenderness 0.3.

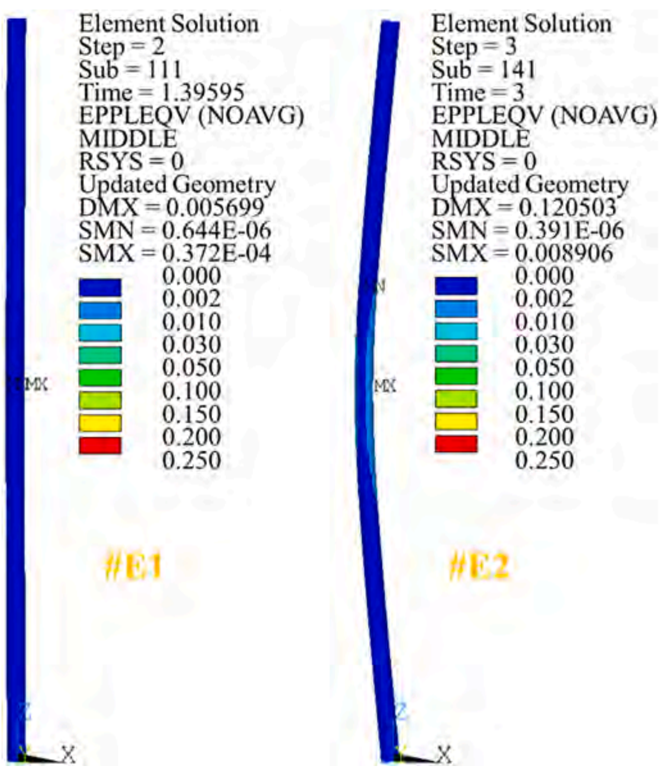


**Fig. 18.** Equivalent plastic strain of column of realization (#LN) with the highest $N_u$ value from the group of slenderness 1.2.

presented in the figures in the study of Buchanan et al. [34] (page 308), where the ultimate axial load normalized by the yield load $N_u/(A\,\sigma_{0.2})$ is determined for various slenderness values, utilizing results of FE analysis of various CHS geometries. There does not seem to be an evident pattern of different CHS geometries other than the mentioned exclusion of cross-sectional class 4 [11] from the data set, as for the 4th cross-sectional class, the effective area $A_{eff}$ is used instead of the original cross-sectional area $A$ [11], and the normalization of the cross-sectional class 4 denoted as $N_u/(A_{eff}\,\sigma_{0.2})$ would result in particularly conservative resistance [34]. Therefore, for the CHS of cross-sections with a larger ratio of $D/t$ (diameter to thickness), such as the cross-sectional classes 4 [11], it might be more important to also introduce local geometrical imperfection (which has been neglected in this study).

The material type of the stainless steel has a more significant influence on the suitability of the utilized values of the imperfection factor $\alpha$ and the limit slenderness $\bar{\lambda}_0$. The results of this study are limited to austenitic (normal strength) stainless steel. For example, the behaviour of duplex stainless steel CHS members is better predicted by the existing EN 1993-1-4 [11] buckling curve, as discussed by Buchanan et al. [34] or Ellobody and Young [18].

### 7.2. Design provisions of flexural buckling resistance of austenitic CHS members

The EC 3 design method of predicting the flexural buckling resistance of the austenitic stainless steel (grade EN 1.4307) CHS columns does not fulfil the required safety level (probability of failure $7.2 \cdot 10^{-5}$) of the EC 0 requirements for members of relative slenderness $\bar{\lambda}$ approximately in the range 0.2–0.9 (Fig. 8). This observation corresponds to similar previous research studies [12–19].

Proposed improvements: If the design provisions proposed by Buchanan et al. [34] are considered during the calculation of the flexural buckling design resistance value, the results fulfil the safety requirements for all but one of the analysed $\bar{\lambda}$ values (Fig. 8). Only the design resistance based on FORM for approach #G and the relative slenderness of $\bar{\lambda} = 0.69$ is noticeably below the resistance-slenderness curve ($\bar{\lambda}_0 = 0.2$) [34]. For this case, however, the standard skewness and standard kurtosis (Table 4) are of relatively high values, which indicates an increased statistical error. Moreover, the results of approach #G use more conservative values of the initial geometrical imperfection $e_0$, as well as its statistical distribution parameters. The values of $e_0$ based on the recent statistical research [40] are used in the approach #LN. The results of the #G approach are overall more conservative.

### 7.3. Correlations between the ultimate resistance and input parameters

The highest influence of $e_0$ on the ultimate resistance $N_u$ (in the matter of linear correlation) is observed for slenderness values around $\bar{\lambda} = 1.20$ (Fig. 9 and Fig. 10). A higher coefficient of correlation between $N_u$ and $e_0$ is achieved for the #G approach, as the standard deviation for $e_0$ was considered larger than in the #LN approach. The correlations between $N_u$ and 0.2% proof stress $\sigma_{0.2}$, ultimate stress $\sigma_u$, and strain $\varepsilon_u$ are much higher for smaller values of slenderness. For large slenderness values, global buckling and therefore the ultimate resistance $N_u$ is achieved before the stresses in the member reach the material 0.2% proof stress (alternative to the yield strength for the stainless steel material).

The highest value of the correlation through all the analysed slenderness values is observed between $N_u$ and the tube wall thickness $t$. Thickness has, of course, a high impact on the cross-section area. During the manufacturing process, it is much easier to produce a CHS member of a certain diameter $D$ than of a given thickness $t$, as it is evident in the coefficient of variation for these geometrical parameters (CoV of the thickness $t$ is much higher than CoV of the diameter $D$). The correlation between $N_u$ and $D$ is small but positive, sometimes rather negligible for all the slenderness values.

With higher slenderness values, the correlation between $N_u$ and Young's modulus $E$ increases. The behaviour of members of large slenderness is more similar to strings than columns in compression, the ultimate resistance force is closer to estimations based on the well known Euler critical force $N_{cr}$ (graphically converges to the Euler hyperbole) (Fig. 8):

$$N_{cr} = \frac{\pi^2 \bullet E \bullet I}{(\beta_{cr} \bullet L)^2} \tag{24}$$

where $\beta_{cr}$ is the effective length factor (for the pin-ended column equal to 1.0). Global stability loss occurs before the material yield strength is reached. The major factors influencing the ultimate resistance, or equivalently the critical force $N_{cr}$ for large slenderness (except for the length $L$ with its negligible standard deviation), are the elastic modulus $E$ and the second moment of area $I$, dependent on the diameter $D$ but more significantly (considering the coefficient of variation) on the thickness $t$.

Only a negligible linear correlation between the structural length $L$ and the ultimate resistance $N_u$ was observed. This is mainly caused by the rather small standard deviation of the column lengths. The correlation balances around the value 0. This correlation is expected negative if the standard deviation of the length $L$ is significant.

The correlation between $N_u$ and the exponent material parameters $m$ and $n$ is more complex to discuss, as both form the shape of the stress-strain relation of the stainless steel material (with the major impact for stresses above the 0.2% proof stress value). The influence of both ($m$ and $n$) is rather negligible for large slenderness values, as the influence of material parameters ($\sigma_{0.2}$, $\sigma_u$, and $\varepsilon_u$) is also rather small, and the only important parameter is the initial slope of the stress-strain curve defined by Young's modulus $E$. The correlation between $N_u$ and $m$ decreases with increasing slenderness values. The correlation between $N_u$ and $n$ is less monotonous, with negative values for little slenderness, the highest positive values for slenderness around 1.0–1.1, and decreasing again for large slenderness.

### 7.4. Amount of the plastic strain at ultimate resistance for slender and less slender members

An example of the equivalent plastic strain of higher slenderness cases is depicted in Fig. 15 (slenderness 1.1, modelling approach #G) and Fig. 18 (slenderness 1.2, approach #LN). The points of the ultimate resistances are #C1 (Fig. 15) and #E1 (Fig. 18). The plasticity at the ultimate resistance of the columns of higher slenderness values is rather negligible also if the initial global geometrical imperfection $e_0$ is very close to 0 (#C1 in Fig. 15). Equivalent plastic strains at the ultimate resistance point of smaller slenderness columns reach values higher than 0.2% (therefore the stress is above the 0.2% proof stress value). An example for slenderness 0.3 is in Fig. 17 (#D1), or for a very small $e_0$ value in Fig. 13 (#A1) and Fig. 14 (#B1, slenderness 0.2). This corresponds with the increasing correlation between the ultimate resistance $N_u$ and 0.2% proof stress $\sigma_{0.2}$ for less slender members, as discussed in chapter 7.3, and depicted in Fig. 9 and Fig. 10.

### 7.5. Failure modes

In general, the most common failure mode was the global stability loss, which by its shape resembles the lowest eigenvalue shape of the modal analysis. An example is shown in Fig. 18 (#E2) for the slenderness 1.2, or in Fig. 15 (#C2) for the slenderness 1.1.

Additionally, columns of smaller slenderness developed a local stability loss at the compressed side in the mid-height generally sooner (in the matter of decreasing value of the axial load $N_z$ after the curve peak, the ultimate resistance $N_u$ was reached). This is visible in the more sudden tangent change of the decreasing curves. For example, for the slenderness of 0.3 (Fig. 16), this occurred at the $N_z$ value (corresponding to $u_x$ of circa 25 mm) which is relatively much closer to $N_u$ than for the slenderness 1.1 (Fig. 11), where this occurred at $N_z$ value (at $u_x$ of approx. 200 mm), which is further from the ultimate resistance (the curve peak) of that case.

### 7.6. Small values of the initial geometrical imperfection

In few realizations with very small initial geometrical imperfection value $e_0$ (essentially almost zero value), the so-called "elephant foot" shape of the local stability loss developed near the end parts of the column. This occurred for small slenderness, exclusively. An example for the slenderness 0.2 is depicted in Fig. 14 (full circumference elephant foot), or for the slenderness 0.3, where the local stability loss occurred at the column ends only partially (not along the whole circumference), and also in the mid-height. The horizontal deflections of this case are also unique in the matter of initially opposite direction than the direction of the applied geometrical imperfection $e_0$ (Fig. 12 #A0). The value of $e_0$ was very close to 0, and this behaviour might also be influenced by the numerical rounding during the analysis. Such behaviour was very rare and only occurred for a few cases of small slenderness with a very small $e_0$ value (therefore only in the #G modelling approach).

This shape of deformation, when a ring-like bulge is formed near one or both ends of the column (elephant foot buckling) is a very common local failure shape for compressed members of tubular cross-sections [29,34,75], and the most common shape for specimens with very low imperfections [76]. An example of this local failure mode after the physical experiment is shown in Fig. 19, where very short stub column test specimens were exposed to a compressive load in a study by Zhang et al. [5].

### 7.7. Initial geometrical imperfection provisions

If the quality of production follows the statistical characteristics of the initial imperfection $e_0$ [40], then the new tolerance limits $L/1666$ could be considered in both metallurgical production and stochastic models. Compared to carbon steel, stainless steel products have different geometric and material characteristics, thus new research using updated probabilistic analysis [46,77] and new types of reliability-oriented sensitivity analysis can be done [52,78,79].

## 8. Conclusion

Advanced finite element modelling was used to investigate the flexural buckling resistance of circular hollow section (CHS) austenitic stainless steel columns of 15 different relative slenderness $\overline{\lambda}$ within the range 0.2–1.8.

Two sets of distributions of the initial geometrical imperfection amplitude $e_0$ were introduced, the lognormal and normal (Gauss), here referred to as the #LN and the #G approach respectively. For the #G approach, the mean value of the initial geometrical imperfection was equal to 0, and there was a higher standard deviation compared to the approach #LN, where a non-zero mean value of the imperfection was utilized along with a smaller standard deviation.

In order to determine the design resistances of the columns in flexural buckling based on the geometrically and materially nonlinear imperfect FEM analyses (GMNIA), the EC 0 approach of the first-order


**Fig. 19.** Example of deformed CHS stub column test specimens after physical experiment [5].

reliability method (FORM) was adopted. The resistances determined this way are practically the same as the 0.1% quantile of the Gauss distribution of the ultimate resistances $N_u$.

The Eurocode 3 design values of the flexural buckling resistance (EC 3) are in good agreement with the resistance values utilizing the FORM for the column slenderness above 1.40 for both presented approaches #LN and #G (Fig. 8).

For the #LN approach, the EC 3 results are conservative for the slenderness values between 1.0 and 1.4 compared to the 0.1% quantile, however, the Eurocode design resistances tend to be rather non-conservative for the CHS columns of slenderness around 0.8, and even more unsafe for smaller slenderness values around 0.4–0.5.

The results of the flexural resistance based on the #G approach follow a very similar pattern as the results of the #LN approach. In general, design resistances based on the #G approach are slightly more conservative for slenderness in the interval 0.4–1.4.

The EC 3 approach using the design provisions recommended by Buchanan et al. [34] is much closer to the results based on FORM for smaller slenderness 0.2–0.6 (Fig. 8), more conservative for relative slenderness values $\overline{\lambda}$ around 1.0 and practically the same for large slenderness values. The only alternation proposed by this approach was to use the relative limit slenderness value of $\overline{\lambda}_0 = 0.2$ [34] instead of 0.4, which is currently defined by the EC 3 [11]. The value of 0.4 seems to be rather unsafe for austenitic stainless steel CHS members of the relative slenderness values in the range 0.2–1.0, for the CHS 80 × 1.5 (as analysed in this study), with practically the same performance expectations for the CHS members of cross-sectional classes 1, 2 and 3 defined by EC 3 [11]. The implementation of this design approach by Buchanan et al. [34] into the EC 3 can be recommended. This design approach was chosen from the other proposed approaches and tested in this paper due to its simpler implementation into the current standards for the design of stainless steel (EC 3).

## CRediT authorship contribution statement

**Daniel Jindra**: Conceptualization, Methodology, Formal analysis, Writing-original draft, Visualization, Resources, Investigation, Writing-Review and Editing. **Zdenek Kala**: Conceptualization, Methodology, Methodology of reliability analysis, Supervision, Writing-Review and Editing, Project administration, Funding acquisition. **Jiri Kala**: Conceptualization, Methodology, Writing-Review and Editing, Supervision, Data Curation.

## Declaration of Competing Interest

The authors declare that they have no known competing financial interests or personal relationships that could have appeared to influence the work reported in this paper.

## Acknowledgements

This paper was created with the financial support of Czech Science Foundation by project No.: 20−00761S "Influence of material properties of stainless steels on reliability of bridge structures". Another financial support was provided by the Brno University of Technology fund for specific university research, the project number FAST-J-21-7169.

## References

[1] M.F. Hassanein, M. Elchalakani, A. Karrech, V.I. Patel, E. Dacher, Finite element modelling of concrete-filled double-skin short compression members with CHS outer and SHS inner tubes, Mar. Struct. 64 (2018) 85–99, https://doi.org/10.1016/j.marstruc.2018.05.002.

[2] L. Gardner, The use of stainless steel in structures, Prog. Struct. Eng. Mater. 7 (2) (2005) 45–55, https://doi.org/10.1002/pse.190.

[3] J.A. Sobrino, Stainless steel road bridge in Menorca, Spain, Struct. Eng. Int. 16 (2) (2006) 96–100, https://doi.org/10.2749/101686606777962585.

[4] S.M. Daghash, Q. Huang, O.E. Ozbulut, Tensile behavior and cost-efficiency evaluation of ASTM A1010 steel for bridge construction, J. Bridg. Eng. 24 (8) (2019), 04019078, https://doi.org/10.1061/(ASCE)BE.1943-5592.0001449.

[5] R. Zhang, L. Gardner, C. Buchanan, V.P. Matilainen, H. Piili, A. Salminen, Testing and analysis of additively manufactured stainless steel CHS in compression, Thin-Walled Struct. 159 (2021) 107270, https://doi.org/10.1016/j.tws.2020.107270.

[6] A. He, Y. Sun, N. Wu, O. Zhao, Testing, simulation and design of eccentrically loaded austenitic stainless steel CHS stub columns after exposure to elevated temperatures, Thin-Walled Struct. 164 (2021) 107885, https://doi.org/10.1016/j.tws.2021.107885.

[7] A.D. Martins, R. Goncalves, D. Camotim, Numerical simulation and design of stainless steel columns under fire conditions, Eng. Struct. 229 (2021) 111628, https://doi.org/10.1016/j.engstruct.2020.111628.

[8] A. Mohammed, K.A. Cashell, Structural behaviour and fire design of duplex and ferritic stainless steel CHS stub columns, Int. J. Steel Struct. 21 (2021) 1280–1291, https://doi.org/10.1007/s13296-021-00502-0.

[9] A. Mohammed, S. Afshan, Numerical modelling and fire design of stainless steel hollow section columns, Thin-Walled Struct. 144 (1–13) (2019) 106243, https://doi.org/10.1016/j.tws.2019.106243.

[10] A. He, H.T. Li, X. Lan, Y. Liang, O. Zhao, Flexural buckling behaviour and residual strengths of stainless steel CHS columns after exposure to fire, Thin-Walled Struct. 152 (2020) 106715, https://doi.org/10.1016/j.tws.2020.106715.

[11] European Committee for Standardization, EN 1993-1-4:2006+A1:2015, Eurocode 3 — Design of Steel Structures — Part 1–4: General rules — Supplementary rules for Stainless Steels, CEN, Brussels, Belgium, 2015.

[12] B. Young, W. Hartono, Compression tests of stainless steel tubular members, J. Struct. Eng. 128 (6) (2002) 754–761, https://doi.org/10.1061/(ASCE)0733-9445(2002)128:6(754).

[13] K.J.R. Rasmussen, J. Rondal, Column curves for stainless steel alloys, J. Constr. Steel Res. 54 (1) (2000) 89–107, https://doi.org/10.1016/S0143-974X(99)00095-4.

[14] M. Ashraf, L. Gardner, D.A. Nethercot, Resistance of stainless steel CHS columns based on cross-section deformation capacity, J. Constr. Steel Res. 64 (9) (2008) 962–970, https://doi.org/10.1016/j.jcsr.2007.10.010.

[15] M. Theofanous, T.M. Chan, L. Gardner, Structural response of stainless steel oval hollow section compression members, Eng. Struct. 31 (4) (2009) 922–934, https://doi.org/10.1016/j.engstruct.2008.12.002.

[16] G. Shu, B. Zheng, L. Xin, A new design method for stainless steel columns subjected to flexural buckling, Thin-Walled Struct. 83 (2014) 43–51, https://doi.org/10.1016/j.tws.2014.01.018.

[17] B. Young, E. Ellobody, Column design of cold-formed stainless steel slender circular hollow sections, Steel Compos. Struct. 6 (4) (2006) 285–302, https://doi.org/10.12989/scs.2006.6.4.285.

[18] E. Ellobody, B. Young, Investigation of cold-formed stainless steel non-slender circular hollow section columns, Steel Compos. Struct. 7 (4) (2007) 321–337, https://doi.org/10.12989/scs.2007.7.4.321.

[19] K. Ning, L. Yang, J. Wang, P. Dai, Y. Sun, Experimental and numerical study of hot-rolled duplex stainless steel CHS columns, J. Constr. Steel Res. 180 (2021) 106579, https://doi.org/10.1016/j.jcsr.2021.106579.

[20] S. Afshan, B. Rossi, L. Gardner, Strength enhancements in cold-formed structural sections - part I: material testing, J. Constr. Steel Res. 83 (2013) 177–188, https://doi.org/10.1016/j.jcsr.2012.12.008.

[21] K.J.R. Rasmussen, G.J. Hancock, Design of cold-formed stainless steel tubular members. I: columns, J. Struct. Eng. 119 (8) (1993) 2349–2367, https://doi.org/10.1061/(ASCE)0733-9445(1993)119:8(2349.

[22] A. Talja, Test Report on Welded I and CHS Beams, Columns and Beam-Columns, Report to ECSC VTT Building Technology, Technical Research Centre of Finland (VTT), Espoo, Finland, 1997.

[23] B.A. Burgan, N.R. Baddoo, K.A. Gilsenan, Structural design of stainless steel members - comparison between Eurocode 3, Part 1.4 and test results, J. Constr. Steel Res. 54 (1) (2000) 51–73, https://doi.org/10.1016/S0143-974X(99)00055-3.

[24] K.J.R. Rasmussen, Recent research on stainless steel tubular structures, J. Constr. Steel Res. 54 (1) (2000) 75–88, https://doi.org/10.1016/S0143-974X(99)00052-8.

[25] H. Kuwamura, Local buckling of thin-walled stainless steel members, Int. J. Steel Struct. 3 (2003) 191–201.

[26] L. Gardner, D.A. Nethercot, Experiments on stainless steel hollow sections - part 1: material and cross-sectional behaviour, J. Constr. Steel Res. 60 (9) (2004) 1291–1318, https://doi.org/10.1016/j.jcsr.2003.11.006.

[27] D. Lam, L. Gardner, Structural design of stainless steel concrete filled columns, J. Constr. Steel Res. 64 (11) (2008) 1275–1282, https://doi.org/10.1016/j.jcsr.2008.04.012.

[28] B. Uy, Z. Tao, L.H. Han, Behaviour of short and slender concrete-filled stainless steel tubular columns, J. Constr. Steel Res. 67 (3) (2011) 360–378, https://doi.org/10.1016/j.jcsr.2010.10.004.

[29] O. Zhao, L. Gardner, B. Young, Structural performance of stainless steel circular hollow sections under combined axial load and bending - part 1: experiments and numerical modelling, Thin-Walled Struct. 101 (2016) 231–239, https://doi.org/10.1016/j.tws.2015.12.003.

[30] O. Zhao, L. Gardner, B. Young, Testing and numerical modelling of austenitic stainless steel CHS beam-columns, Eng. Struct. 111 (2016) 263–274, https://doi.org/10.1016/j.engstruct.2015.12.035.

[31] F.C. Bardi, S. Kyriakides, Plastic buckling of circular tubes under axial compression - part I: experiments, Int. J. Mech. Sci. 48 (8) (2006) 830–841, https://doi.org/10.1016/j.ijmecsci.2006.03.005.

[32] J.A. Paquette, S. Kyriakides, Plastic buckling of tubes under axial compression and internal pressure, Int. J. Mech. Sci. 48 (8) (2006) 855–867, https://doi.org/10.1016/j.ijmecsci.2006.03.003.
[33] H. Stangenberg, Report to the ECSC - Draft Final Report Ferritic Stainless Steels, Tech. Rep.; RWTH, 2000.
[34] C. Buchanan, E. Real, L. Gardner, Testing, simulation and design of cold-formed stainless steel CHS columns, Thin-Walled Struct. 130 (2018) 297–312, https://doi.org/10.1016/j.tws.2018.05.006.
[35] C. Buchanan, O. Zhao, E. Real, L. Gardner, Cold-formed stainless steel CHS beam-columns — Testing, simulation and design, Eng. Struct. 213 (2020), https://doi.org/10.1016/j.engstruct.2020.110270.
[36] Y. Xu, M. Zhang, B. Zheng, Design of cold-formed stainless steel circular hollow section columns using machine learning methods, Struct. 33 (2021) 2755–2770, https://doi.org/10.1016/j.istruc.2021.06.030.
[37] Y.X. Ma, K.H. Tan, A unified approach for austenitic and ferritic stainless steel CHS beam–columns subjected to eccentric loading, Thin-Walled Struct. 165 (2021) 107918, https://doi.org/10.1016/j.tws.2021.107918.
[38] Ansys, Inc, ANSYS 20.0, Ansys, Inc., Canonsburg, PA, USA, 2019.
[39] European Committee for Standardization, EN 1990:2002+A1:2005 (E), Eurocode 0: Basis of structural design, in: CEN, Brussels, Belgium, 2005.
[40] I. Arrayago, K.J. Rasmussen, E. Real, Statistical analysis of the material, geometrical and imperfection characteristics of structural stainless steels and members, J. Constr. Steel Res. 175 (2020) 106378, https://doi.org/10.1016/j.jcsr.2020.106378.
[41] S. Chen, C. Hou, H. Zhang, L.H. Han, Ting-Min Mud, Reliability-based evaluation for concrete-filled steel tubular (CFST) truss under flexural loading, J. Constr. Steel Res. 169 (2020) 106018, https://doi.org/10.1016/j.jcsr.2020.106018.
[42] S. Chen, C. Hou, H. Zhang, L.H. Han, Structural behavior and reliability of CFST trusses with random initial imperfections, Thin-Walled Struct. 143 (2019) 106192, https://doi.org/10.1016/j.tws.2019.106192.
[43] European Committee for Standardization, EN 10088–4:2009, Stainless Steels Part 4: Technical Delivery Conditions for Sheet/Plate and Strip of Corrosion Resisting Steels for Construction Purposes, CEN, Brussels, Belgium, 2009.
[44] M.H. Faber, Statistics and probability theory: In Pursuit of Engineering Decision Support, (Part of the Topics in Safety, Risk, Reliability and Quality, book series TSRQ, volume 18), Springer Publishing Company (2012) 192. eISBN: 978-94-007-4056-3. doi:https://doi.org/10.1007/978-94-007-4056-3.
[45] Y.G. Zhao, T. Ono, A general procedure for first/second-order reliability method (FORM/SORM), Struct. Saf. 21 (1999) 95–112.
[46] J. Jönsson, M.S. Müller, Ch. Gamst, J. Valeš, Z. Kala, Investigation of European flexural and lateral torsional buckling interaction, J. Constr. Steel Res. 156 (2019) 105–121, https://doi.org/10.1016/j.jcsr.2019.01.026.
[47] Z. Kala, From probabilistic to quantile-oriented sensitivity analysis: New indices of design quantiles, Symmetry 12 (10) (2020) 1720, https://doi.org/10.3390/sym12101720.
[48] Z. Kala, Sensitivity analysis in probabilistic structural design: A comparison of selected techniques, Sustainability 12 (11) (2020) 4788, https://doi.org/10.3390/su12114788.
[49] Z. Kala, J. Valeš, J. Jönsson, Random fields of initial out of straightness leading to column buckling, J. Civ. Eng. Manag. 23 (7) (2017) 902–913, https://doi.org/10.3846/13923730.2017.1341957.
[50] Z. Kala, Quantile-oriented global sensitivity analysis of design resistance, J. Civ. Eng. Manag. 25 (4) (2019) 297–305, https://doi.org/10.3846/jcem.2019.9627.
[51] Z. Kala, Quantile-based versus Sobol sensitivity analysis in limit state design, Structures. 28 (2020) 2424–2430, https://doi.org/10.1016/j.istruc.2020.10.037.
[52] Z. Kala, Global sensitivity analysis of quantiles: New importance measure based on superquantiles and subquantiles, Symmetry 13 (2) (2021) 263, https://doi.org/10.3390/sym13020263.
[53] Z. Kala, J. Melcher, L. Puklický, Material and geometrical characteristics of structural steels based on statistical analysis of metallurgical products, J. Civ. Eng. Manag. 15 (3) (2009) 299–307, https://doi.org/10.3846/1392-3730.2009.15.299-307.
[54] D. Jindra, Z. Kala, J. Kala, Validation of stainless-steel CHS columns finite element models, Materials. 14 (7) (2021) 1785, https://doi.org/10.3390/ma14071785.
[55] British Standards Institution, BS EN 1090-2:2008+A1:2011, Execution of steel structures and Aluminum Structures - Technical Requirements for Steel Structures, in: BSI, London, UK, 2008.
[56] American Institute of Steel Construction (AISC), Specification for Structural Steel Buildings (AISC 360–10), AISC, Chicago, Illinois, 2010.
[57] Ministry of Housing and Urban-Rural Development of the People"s Republic of China, Standard for Design of Steel Structures: GB50017–2017, China Architecture & Building Press, Beijing, 2017.
[58] X. Yang, Y. Xiang, Y.F. Luo, X.N. Guo, J. Liu, Axial compression capacity of steel circular tube with large initial curvature: Column curve and application in structural assessment, J. Constr. Steel Res. 177 (2021) 106481, https://doi.org/10.1016/j.jcsr.2020.106481.
[59] J. Jönsson, T.C. Stan, European column buckling curves and finite element modelling, J. Construct. Steel Res. 128 (2017) 136–151, https://doi.org/10.1016/j.jcsr.2016.08.013.
[60] Z. Kala, J. Valeš, Imperfection sensitivity analysis of steel columns at ultimate limit state, Arch. Civ. Mech. Eng. 18 (2018) 1207–1218, https://doi.org/10.1016/j.acme.2018.01.009.
[61] I. Arrayago, K.J. Rasmussen, Buckling curves for cold-formed stainless-steel columns and beams, J. Struct. Eng. 147 (10) (2021), 04021149, https://doi.org/10.1061/(ASCE)ST.1943-541X.0003084.
[62] W. Ramberg, W.R. Osgood, Description of Stress-Strain Curves by Three Parameters, Technical Note No. 902, National Advisory Committee for Aeronautics, Washington, DC, USA, 1943.
[63] H.N. Hill, Determination of Stress-Strain Relations from the Offset Yield Strength Values; Technical Note No. 927, National Advisory Committee for Aeronautics, Washington, DC, USA, 1944.
[64] L. Gardner, D.A. Nethercot, Numerical modelling of cold-formed stainless steel sections, in: Proceedings of the NSCC 2001, 9th Nordic Steel Construction Conference, Helsinki, Finland, 18–20 June 2001, Helsinki University of Technology, Helsinki, Finland, 2001, pp. 781–789.
[65] E. Mirambell, E. Real, On the calculation of deflections in structural stainless steel beams: An experimental and numerical investigation, J. Constr. Steel Res. 54 (1) (2000) 109–133, https://doi.org/10.1016/S0143-974X(99)00051-6.
[66] D. Jindra, Z. Kala, S. Seitl, J. Kala, Material model parameter identification of stainless steel (AISI 304L), in: V. Fuis (Ed.), Proceedings of the Engineering Mechanics 2020, Institute of Theoretical and Applied Mechanics of the Czech Academy of Sciences—AS CR: Brno, Czech Republic, 2020, pp. 246–249, in: https://www.engmech.cz/improc/2020/246.pdf.
[67] R.B. Cruise, L. Gardner, Residual stress analysis of structural stainless steel sections, J. Constr. Steel Res. 64 (2008) 352–366, https://doi.org/10.1016/j.jcsr.2007.08.001.
[68] M. Jandera, L. Gardner, J. Machacek, Residual stresses in cold-rolled stainless steel hollow sections, J. Constr. Steel Res. 64 (11) (2008) 1255–1263, https://doi.org/10.1016/j.jcsr.2008.07.022.
[69] Z. Kala, Sensitivity and reliability analysis of lateral-torsional buckling resistance of steel beams, Arch. Civ. Mech. Eng. 15 (4) (2015) 1098–1107, https://doi.org/10.1016/j.acme.2015.03.007.
[70] D.E. Hungtington, C.S. Lyrintzis, Improvements to and limitations of Latin hypercube sampling, Probabilistic. Eng. Mech. 13 (4) (1998) 245–253, https://doi.org/10.1016/S0266-8920(97)00013-1.
[71] M.D. McKay, R. Beckman, W. Conover, A comparison of three methods for selecting values of input variables in the analysis of output from a computer code, Technometrics 21 (2) (1979) 239–245, https://doi.org/10.1080/00401706.1979.10489755.
[72] R.L. Iman, W.J. Conover, A distribution-free approach to inducing rank correlation among input variables, Commun. Stat. Simul. Comput. 11 (3) (1982) 311–334, https://doi.org/10.1080/03610918208812265.
[73] GmbH Dynardo, OptiSLang Software Manual: Methods for Multi-Disciplinary Optimization and Robustness Analysis, Weimar. https://www.ansys.com/products/platform/ansys-optislang, 2019.
[74] K. Pearson, X. On the criterion that a given system of deviations from the probable in the case of a correlated system of variables is such that it can be reasonably supposed to have arisen from random sampling, in: The London, Edinburgh and Dublin Philosophical Magazine and Journal of Science Series 5 50(302), 1900, pp. 157–175, https://doi.org/10.1080/14786440009463897.
[75] C. Buchanan, V.P. Matilainen, A. Salminen, L. Gardner, Structural performance of additive manufactured metallic material and cross-sections, J. Constr. Steel Res. 136 (2017) 35–48, https://doi.org/10.1016/j.jcsr.2017.05.002.
[76] A. Insausti, L. Gardner, Analytical modelling of plastic collapse in compressed elliptical hollow sections, J. Constr. Steel Res. 67 (4) (2011) 678–689, https://doi.org/10.1016/j.jcsr.2010.11.012.
[77] Z. Kala, Reliability analysis of the lateral torsional buckling resistance and the ultimate limit state of steel beams with random imperfections, J. Civ. Eng. Manag. 21 (7) (2015) 902–911, https://doi.org/10.3846/13923730.2014.971130.
[78] Z. Kala, Global sensitivity analysis based on entropy: From differential entropy to alternative measures, Entropy 23 (6) (2021) 778, https://doi.org/10.3390/e23060778.
[79] Z. Kala, New importance measures based on failure probability in global sensitivity analysis of reliability, Mathematics 9 (19) (2021) 2425, https://doi.org/10.3390/math9192425.